# Finite-size effect on the surface deformation thermal mirror method

**N. G. C. Astrath,[1,*] L. C. Malacarne,[1,3] V. S. Zanuto,[1] M. P. Belancon,[1] R. S. Mendes,[1] M. L. Baesso,[1] and C. Jacinto[2]**

[1]*Grupo de Estudo dos Fenômenos Fototérmicos, Departamento de Física, Universidade Estadual de Maringá, Maringá—PR, 87020-900, Brasil*

[2]*Grupo de Fotônica e Fluidos Complexos, Instituto de Física, Universidade Federal de Alagoas, Maceiô—AL, 57072-970, Brazil*

[3]*e-mail: lcmala@pq.cnpq.br*

**Corresponding author: astrathngc@pq.cnpq.br*

Received May 11, 2011; accepted May 20, 2011;
posted May 26, 2011 (Doc. ID 147435); published June 23, 2011

The finite-size effect on the thermal mirror (TM) experiments is described. The time-resolved thermoelastic deformation equation is solved and compared to the semi-infinite solution. To determine the applicability of the semi-infinite model, experiments were performed in optical glasses and the quantitative results compared to both models. The analytical results presented here were found to be in excellent agreement with the numerical finite elemental analysis model. Modeling and experiment showed that the TM transient signal is strongly affected as the sample thickness is reduced. The results of the finite-size model demonstrate that it is intrinsically more accurate to characterize physical properties of low optical absorption thin samples, which suggests that the model and the TM method could even be applied to study very thin films down to the micrometer scale. 

*OCIS codes:* 140.6810, 350.5340, 300.6430.

## 1. INTRODUCTION

Photothermal displacement techniques are powerful tools for material characterization [1–3]. These methods have been theoretically and experimentally developed over the past few decades and attracted great interest in many research aspects, such as nondestructive evaluation of solids, surfaces, multilayered, and thin films; semiconductors; and biological ablation under modulated [4–11] and pulsed [12–14] laser excitations. The basic principle, employed in almost all studies to date, consists of detecting the laser-induced surface deformation of a solid sample. The deformation of the sample can be detected by deflection or focusing/defocusing of the probe beam reflected from the sample surface, interferometric methods, or an attenuated total reflection scheme. The fast, noncontacting, and highly sensitive detection characteristics of these methods are very useful for studying low optical absorbing to opaque solids.

A time-resolved photothermal deformation method, namely thermal mirror (TM), has been introduced under cw Gaussian [15–17] and top-hat [18,19] laser excitations. Thermal diffusivity and thermo-optical properties were quantitatively determined for semitransparent and opaque solids. It was also concurrently used with the thermal lens method to determine physical properties of fluorescent materials [18]. The TM effect arises from a local surface deformation of the sample, created by the temperature rise produced by absorbance of a laser beam (excitation laser). Another Gaussian beam, almost collinearly arranged with the excitation beam, impinges the excited area and the center point of the spot of its reflection is probed in the far-field region.

The TM theoretical model for both the Gaussian and the top-hat excitations were developed assuming the sample as a semi-infinite medium and the thermoelastic equations were solved accordingly [17]. Under the semi-infinite approximation, the sample is treated as an infinite medium along the $z$ axis with its surface placed at $z = 0$. This assumption reduces the boundary conditions over the stress components to the free surface only at $z = 0$. In other words, it is assumed that the thickness is large enough that the displacement vector at the surface is not affected by the induced deformation within the sample at $z = l$, with $l$ being the sample thickness. However, the minimum thickness required to fulfill this approach depends on the thermo-optical and mechanical properties of the sample and cannot be determined using the semi-infinite model. Here we show that the size effect should be considered for thin samples. In this work, we present a theoretical and experimental analysis of the surface deformation in a finite-size model. We used the analytical solutions for the thermoelastic deformation under Gaussian laser excitation for low optical absorbing samples to model the TM effect and the results are compared with the numerical finite elemental analysis (FEA). The FEA modeling results are found to be in excellent agreement with the analytical solutions. Experiments are performed in optical glasses and the results are analyzed with the finite and semi-infinite models. The limits of application of both models are investigated.

## 2. THEORY

We used the TM technique in a mode-mismatched configuration. In this configuration, a sample of thickness $l$ is excited

 

and probed by cw $TEM_{00}$ Gaussian beams with radii $\omega$ and $\omega_{1P}$, respectively [17].

The thermoelastic equation for the surface displacement caused by a laser-induced nonuniform temperature distribution, in the quasi-static approximation, can be expressed in cylindrical coordinates due to the geometry of the Gaussian pump laser beam by introducing the scalar displacement potential $\Psi$ and the Love function $\psi$ following by the Poisson's equation,

$$\nabla^2\Psi(r,z,t)=\frac{1+\nu}{1-\nu}\alpha_T T(r,z,t), \tag{1}$$

and the biharmonic equation,

$$\nabla^2\nabla^2\psi(r,z,t)=0. \tag{2}$$

$\alpha_T$ is the linear thermal expansion coefficient and $\nu$ the Poisson's ratio [20]. $r$ is the radial coordinate and $t$ is the time. The components $r$ and $z$ of the displacement vector ($u_r$ and $u_z$) and the normal stress components ($\sigma_{zz}$ and $\sigma_{rz}$) are obtained from $\Psi(r,z,t)$ and $\psi(r,z,t)$ by the relations

$$u_i(r,z,t)=\partial_i\Psi(r,z,t)+\frac{1}{1-2\nu}[2(1-\nu)\delta_{zi}\nabla^2 - \partial_{zi}]\psi(r,z,t), \tag{3}$$

$$\sigma_{ij}=2\mu[\partial_{ij}-\delta_{ij}\nabla^2]\Psi(r,z,t) + \frac{2\mu}{1-2\nu}[\partial_z(\nu\delta_{ij}\nabla^2-\partial_{ij}) + (1-\nu)\nabla^2(\delta_{iz}\partial_j+\delta_{jz}\partial_i)]\psi(r,z,t), \tag{4}$$

where $\mu=E/(2+2\nu)$, $E$ is the Young's modulus, $\partial_{ij}$ represents derivatives with respect to $i=r,z$ and $j=r,z$, and $\delta_{ij}$ is the Kronecker delta function. The solution of the Poisson's and biharmonic equations can be written in terms of the Hankel–Fourier transforms of the temperature distribution $T(r,z,t)$, $T(\alpha,\lambda,t)$, as

$$\Psi(r,z,t)=-\frac{1+\nu}{1-\nu}\alpha_T\sqrt{\frac{2}{\pi}}\int_0^\infty\int_0^\infty\frac{T(\alpha,\lambda,t)}{(\alpha^2+\lambda^2)}\mathrm{Cos}(\lambda) \times J_0(\alpha r)\alpha\,\mathrm{d}\alpha\,\mathrm{d}\lambda, \tag{5}$$

$$\psi(r,z,t)=\int_0^\infty[(A+\alpha zB)e^{\alpha z} + (F+\alpha zG)e^{-\alpha z}]\alpha^{-2}J_0(\alpha r)\mathrm{d}\alpha, \tag{6}$$

where $J_n(x)$ represents the Bessel function of the first kind. Assuming free stress boundary conditions at the surfaces $z=0$ and $z=l$, $\sigma_{rz}|_{z=0,l}=0$ and $\sigma_{zz}|_{z=0,l}=0$, the constants $A$, $B$, $F$, and $G$ can be derived, and the displacement at the sample surface, $z=0$, is given as

$$u_z(r,0,t)=\int_0^\infty\frac{2\alpha_T(1+\nu)\alpha^2\vartheta(\alpha,t)J_0(\alpha r)}{1+2l^2\alpha^2-\mathrm{Cosh}(2l\alpha)}\mathrm{d}\alpha, \tag{7}$$

with

$$\vartheta(\alpha,t)=\sqrt{\frac{2}{\pi}}\int_0^\infty\frac{T(\alpha,\lambda,t)}{(\alpha^2+\lambda^2)}\{[2l\alpha+\mathrm{Sinh}(2l\alpha)] - 2[l\alpha\mathrm{Cosh}(l\alpha)+\mathrm{Sinh}(l\alpha)]\mathrm{Cos}(\lambda l) - [2l\mathrm{Sinh}(l\alpha)]\lambda\mathrm{Sin}(\lambda l)\}\mathrm{d}\lambda. \tag{8}$$

In the limit $l\to\infty$ in Eq. (7), the results of [17] for the semi-infinite approximation are recovered.

It is important to note that Eq. (7) works for any cylindrical symmetric heat source, providing $T(\alpha,\lambda,t)$ can be obtained. Although the integrations in Eq. (7) are not straightforward to be performed, $\vartheta(\alpha,t)$ presents an analytical solution when the input temperature is solved for low optical absorbing materials without considering axial heat flux to the surroundings. Specifically for this case, the solution for the heat conduction differential equation in the Hankel–Fourier transform space is [15]

$$T(\alpha,\lambda,t)=\sqrt{2\pi}\frac{Q_0}{c\rho}\delta(\lambda)\frac{\omega^2}{4}e^{-\frac{\omega^2\alpha^2}{8}}\int_0^t e^{-D\alpha^2\tau}\mathrm{d}\tau. \tag{9}$$

The power density factor is $Q_0=2P_eA_e\phi/(\pi\omega^2)$, $\delta(\lambda)$ is the Dirac delta function, and $\rho$ and $c$ are the mass density and specific heat of the sample, respectively. $A_e$ is the optical absorption coefficient of the sample at the excitation wavelength ($\lambda_{ex}$). Using Eq. (9) in Eq. (7), the displacement is

$$u_z(g,0,t)=\theta_{TM}\frac{\lambda_p}{4\pi}\frac{\omega^2}{t_c}\int_0^\infty\frac{\mathrm{Cosh}(l\alpha)-1}{l\alpha+\mathrm{Sinh}(l\alpha)} \times\left(\int_0^t e^{-\frac{\omega^2}{8}\left(1+\frac{2\tau}{t_c}\right)\alpha^2}\mathrm{d}\tau\right)J_0\left(\alpha\omega\sqrt{mg}\right)\mathrm{d}\alpha. \tag{10}$$

$\theta_{TM}=-P_eA_e\alpha_T(1+\nu)\phi/(\lambda_pk)$ is a parameter measuring the strength of the TM effect, $g=(r/\omega_{1p})^2$, and the characteristic heat diffusion time constant is $t_c=\omega^2/(4D)$. $D$ and $k$ are the thermal diffusivity (a measure of the rate of heat transfer) and conductivity of the sample, respectively. $m=(\omega_{1p}/\omega)^2$, $P_e$ is the power of the excitation laser beam, $\lambda_p$ is the probe beam wavelength, and $\phi$ accounts for the fraction of the light energy absorbed not lost by subsequent emission, which is therefore related to the fluorescence quantum efficiency ($\eta$) [18]. Taking the limit $l\to\infty$, Eq. (10) reduces to the displacement profile obtained with the semi-infinite model [17].

The deformation on the sample surface acts as an optical element, causing a phase shift $\Phi_{TM}(r,t)=(4\pi/\lambda_p)[u_z(g,0,t)-u_z(0,0,t)]$ on the reflected part of the probe beam. This phase shift alters the complex amplitude of the electric field propagating to the detector plane, which can be treated as diffraction using Fresnel diffraction theory. Considering only the center of the probe beam spot at the detector plane in the far-field region, its complex amplitude can be written as [17]

$$U(Z_1+Z_2,t)=C\int_0^\infty e^{-(1+iV)g-i\phi_{TM}(g,t)}\mathrm{d}g, \tag{11}$$

where $C$ is a constant [17], $Z_1$ and $Z_2$ are the distances from the probe beam waist to the sample and the sample to the detector plane, respectively, $V=Z_1/Z_C$, and $Z_C$ is the confocal distance of the probe beam. Equation (11) requires numerical integrations over $\alpha$ and $g$. These numerical integrations were

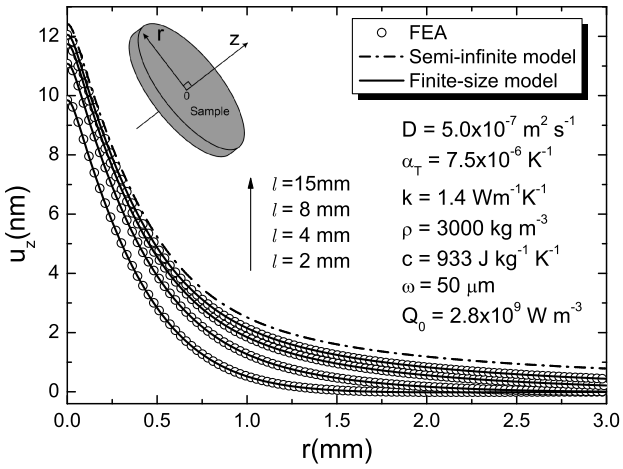


Fig. 1. Displacement profile for a standard glass [21] at $t = 200$ ms using the finite model for different sample thicknesses (solid curves) and the FEA (open circles). Dashed curve represents the semi-infinite solution.

performed using standard commands in Mathematica (version 7.0) software. To reduce the numerical processing time, convergence tests for these integrations were performed and finite values for $\alpha$ and $g$ were defined. In this work, the upper limit of the integrals over $\alpha$ and $g$ were $10^6$ and 25, respectively. The absolute value of the probe beam complex amplitude gives the intensity $I(t)$ at the detector plane as $I(t) = |U(Z_1 + Z_2, t)|^2$.

Figure 1 shows the surface displacement, Eq. (10), calculated with physical parameters of a standard glass [21] using the finite and semi-infinite models, and the corresponding simulation using numerical FEA solution (Comsol Multiphysics software). The physical parameters used in the simulation are displayed in Fig. 1. FEA software provides numerical solutions to the heat transfer equations with the realistic boundary conditions imposed by the experimental geometry; a detailed description of this numerical method is given in [21]. The results show a good agreement between our model and the FEA solutions. In addition, as expected, the finite model solutions approach the semi-infinite one as the sample thickness is increased.

Figure 2 shows TM transient signals calculated using the previous equations for a standard glass [21]. The inset shows the divergence between the parameters $\theta_{TM}$ and $D$ used to simulate the curves, using the finite model, and the respective fits with the semi-infinite model. As expected, the results by the finite model match the semi-infinite one in the large thickness limit.

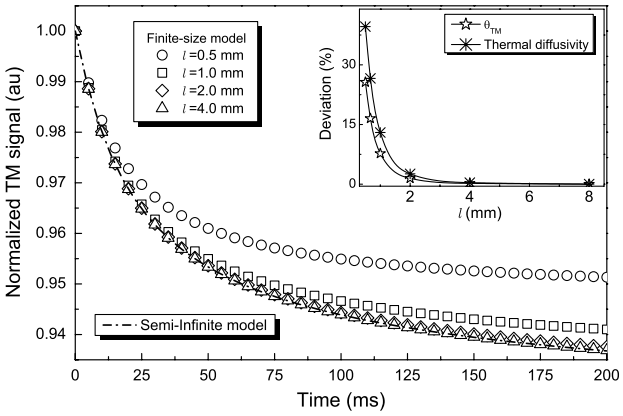


Fig. 2. Simulated TM signal for a standard glass and different thicknesses using the finite model. The inset shows the divergence between the parameters $\theta_{TM}$ and $D$ used to simulate the TM finite model curves and the ones obtained fitting with the semi-infinite model.

## 3. RESULTS AND DISCUSSION

Two samples of different thicknesses ($l = 0.94$ mm and $l = 3.32$ mm) of calcium aluminosilicate glass doped with 2 wt.% $Er_2O_3$ have been used to test the analytical model presented here. The optical absorption coefficient of these samples at $\lambda_{ex} = 488$ nm is approximately 200 m$^{-1}$; this assures that the low optical absorption approximation [15] can be used. The TM experimental apparatus is described in detail in [15,16]. The experimental parameters are shown in Fig. 3(a). It shows typical TM transients for both glasses using an excitation power of $P_e = 550$ mW. The effect of the sample thickness on the TM transient curve can be clearly seen; the amplitude of the TM effect is reduced as the thickness decreases. It can be explained based on the fact that the thinner the sample, the more pronounced the effect of the deformation of the surface $z = l$ over the one at $z = 0$. In other words, the deformation at $z = 0$ is reduced because of the deformation in the opposite direction at $z = l$.

The parameters recovered from the curve fits (solid curves) to the experimental data, using the finite-size model, are the thermal diffusivity $D$ and $\theta_{TM}$. $\theta_{TM}/P_e$ is correlated to the thermal, optical, and mechanical properties of the sample, which are fundamental for material characterization. For instance, it

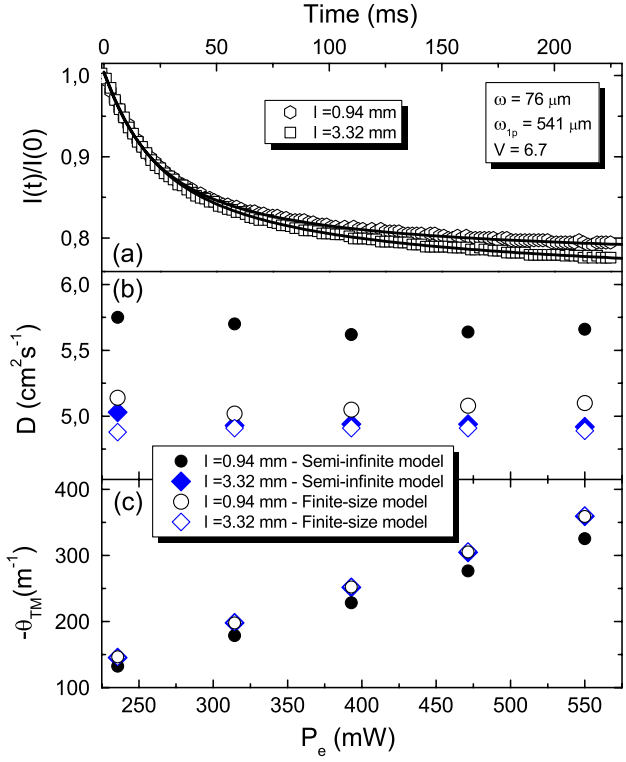


Fig. 3. (Color online) (a) Normalized TM signal, $I(t)/I(0)$, for glass samples; $\lambda_p = 632.8$ nm, $\lambda_{ex} = 488$ nm, and $P_e = 550$ mW. Solid curves represent the theoretical fits using Eq. (10). (b) Thermal diffusivity and (c) $\theta_{TM}$ as a function of the excitation power. The parameters were obtained fitting the experimental transients to the semi-infinite and finite models.

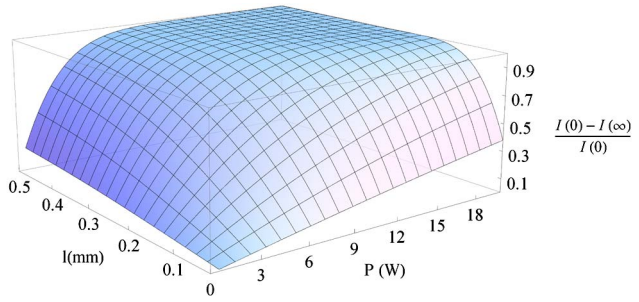


Fig. 4. (Color online) Steady-state TM signal, $[I(0)-I(\infty)]/I(0)$, as function of $P_e$ and $l$. The parameters used in this simulation are listed in Fig. 3, and $\theta_{TM}/P_e = 660\,W^{-1}\,m^{-1}$.

is related with the fluorescence quantum efficiency, which is one of the most important parameters of optical materials [18]. In addition, knowing $\eta$, information of both the thermal expansion coefficient and the Poisson's ratio can be obtained from $\theta_{TM}/P_e$. For the thicker sample, for instance, $D = (4.9 \pm 0.2) \times 10^{-3}\,cm^2\,s^{-1}$ and $\theta_{TM} = (362 \pm 15)\,m^{-1}$, while for the thin one, $D = (5.1 \pm 0.2) \times 10^{-3}\,cm^2\,s^{-1}$ and $\theta_{TM} = (358 \pm 15)\,m^{-1}$. The semi-infinite model was also employed to fit the experimental data. In this way, a comparison between the semi-infinite and finite models can be quantitatively performed.

Figures 3(b) and 3(c) display the fitted parameters obtained by both models for different excitation powers. As one should expect, $\theta_{TM}$ and $D$ obtained for both samples using the finite model are approximately the same. Conversely, the parameters obtained using the semi-infinite model deviate from the ones found using the finite model, mainly for the thin sample. Note that the thick sample falls into the semi-infinite approximation; $\theta_{TM}$ and $D$ are approximately the same as the ones obtained using the finite model. On the other hand, a small systematic error in the $D$ data can be seem in Fig. 3(c) (open symbols) for the two samples, even when the finite model is used. However this difference is less than 3% of the average value of $D$ and is within the experimental error related to the TM technique.

The effect of heat coupling could be eliminated by performing the TM experiments with the sample in a vacuum chamber. In fact, when performed in vacuum, the TM experiments and the finite-size model could be applied to characterize very thin films. The only restriction regarding how thin the sample can be is that high excitation power is needed for thin samples to generate a measurable TM signal. This correlation between excitation power and thickness can be seen in Fig. 4. The amplitude of the TM transient is taken using $I(t)$ in a steady-state regime as the relative signal $[I(0)-I(\infty)]/I(0)$ as a function of excitation power and thickness. This shows that, even for thickness down to a few micrometers, a detectable relative TM signal can be achieved with high excitation powers.

## 4. CONCLUSION

In conclusion, this work describes a theoretical and experimental analysis of the surface deformation in a finite-size TM model. We derived an analytical solutions for the thermoelastic deformation under Gaussian laser excitation for low optical absorbing samples and the results were compared with the numerical FEA solutions. The FEA modeling results were found to be in excellent agreement with the analytical solutions. Experiments were performed in optical glasses and the results were quantitatively analyzed with the finite and semi-infinite models. The experimental results for both the thick and thin samples were the same when the finite model was used and, on the other hand, remained quite different if the semi-infinite model was applied to fit the experimental data. Finally, the TM experimental method and the finite-size model presented here could be applied to study very thin films, down to a few micrometers, providing the experiments are performed in vacuum with high-power excitations. The theory presented here opens up the possibility of extending the modeling to thin films supported on substrates.

## ACKNOWLEDGMENTS

The authors are thankful to the Brazilian Agencies Coordenação de Aperfeiçoamento de Pessoal de Nível Superior, Conselho Nacional de Desenvolvimento Científico e Tecnológico, and Fundação Araucária for the financial support of this work.

## REFERENCES

1. S. E. Bialkowski, *Photothermal Spectroscopy Methods for Chemical Analysis* (Wiley, 1996).
2. A. Mandelis, ed., *Progress in Photoacoustic and Photothermal Science and Technology* (Elsevier, 1991).
3. D. P. Almond and P. M. Patel, *Photothermal Science and Techniques* (Chapman and Hall, 1996).
4. M. A. Olmstead, N. M. Amer, and S. Kohn, "Photothermal displacement spectroscopy—an optical probe for solids and surfaces," Appl. Phys. A **32**, 141–154 (1983).
5. P. Kuo and M. Munidasa, "Single-beam interferometry of a thermal bump," Appl. Opt. **29**, 5326–5331 (1990).
6. J. Cheng and S. Zhang, "3-dimensional theory to study photothermal phenomena of semiconductors. 1. Modulated optical reflectance," J. Appl. Phys. **70**, 6999–7006 (1991).
7. B. C. Li, Z. Zhen, and S. He, "Modulated photothermal deformation in solids," J. Phys. D: Appl. Phys. **24**, 2196–2201 (1991).
8. P. S. Jeon, J. H. Kim, H. J. Kim, and J. Yoo, "The measurement of thermal diffusivities for semi-infinite solids using the photothermal displacement method," Thermochim. Acta **494**, 65–70 (2009).
9. D. Albagli, M. Dark, C. von Rosenberg, L. Perelman, I. Itzkan, and M. S. Feld, "Laser-induced thermoelastic deformation—a 3-dimensional solution and its application to the ablation of biological tissue," Med. Phys. **21**, 1323–1331 (1994).
10. T. Elperin and G. Rudin, "Thermal mirror method for measuring physical properties of multilayered coatings," Int. J. Thermophys. **28**, 60–82 (2007).
11. J. W. Fang and S. Y. Zhang, "Modeling for laser-induced surface thermal lens in semiconductors," Appl. Phys. B **67**, 633–639 (1998).
12. J. C. Cheng, L. Wu, and S. Y. Zhang, "Thermoelastic response of pulsed photothermal deformation of thin plates," J. Appl. Phys. **76**, 716–722 (1994).
13. G. L. Bennis, R. Vyas, R. Gupta, S. Ang, and W. D. Brown, "Thermal diffusivity measurement of solid materials by the pulsed photothermal displacement technique," J. Appl. Phys. **84**, 3602–3610 (1998).
14. B. C. Li, "Three-dimensional theory of pulsed photothermal deformation," J. Appl. Phys. **68**, 482–487 (1990).
15. N. G. C. Astrath, L. C. Malacarne, P. R. B. Pedreira, A. C. Bento, M. L. Baesso, and J. Shen, "Time-resolved thermal mirror for nanoscale surface displacement detection in low absorbing solids," Appl. Phys. Lett. **91**, 191908 (2007).
16. L. C. Malacarne, F. Sato, P. R. B. Pedreira, A. C. Bento, R. S. Mendes, M. L. Baesso, N. G. C. Astrath, and J. Shen, "Nanoscale surface displacement detection in high absorbing solids by time-resolved thermal mirror," Appl. Phys. Lett. **92**, 131903 (2008).
17. F. Sato, L. C. Malacarne, P. R. B. Pedreira, M. P. Belancon, R. S. Mendes, M. L. Baesso, N. G. C. Astrath, and J. Shen,

"Time-resolved thermal mirror method: a theoretical study," J. Appl. Phys. **104**, 053520 (2008).
18. F. B. G. Astrath, N. G. C. Astrath, J. Shen, J. Zhou, L. C. Malacarne, P. R. B. Pedreira, and M. L. Baesso, "Time-resolved thermal mirror technique with top-hat cw laser excitation," Opt. Express **16**, 12214–12219 (2008).
19. N. G. C. Astrath, F. B. G. Astrath, J. Shen, J. Zhou, C. E. Gu, L. C. Malacarne, P. R. B. Pedreira, A. C. Bento, and M. L. Baesso, "Top-hat cw laser induced thermal mirror: a complete model for material characterization," Appl. Phys. B **94**, 473–481 (2009).
20. W. Nowacki, *Thermoelasticity* (Pergamon, 1982).
21. L. C. Malacarne, N. G. C. Astrath, G. V. B. Lukasievicz, E. K. Lenzi, M. L. Baesso, and S. E. Bialkowski, "Time-resolved thermal lens and thermal mirror spectroscopy with sample-fluid heat coupling: a complete model for material characterization," Appl. Spectrosc. **65**, 99–104 (2011).